J. Plasma Phys. (2023), *vol*. 89, 905890410
Published by Cambridge University Press

doi:10.1017/S0022377823000685

Terahertz generation by a rotating relativistic electron beam in a magnetized plasma column

Devki Nandan Gupta,†, **Mukesh Chand Gurjar** and **Arohi Jain**

Department of Physics and Astrophysics, University of Delhi, Delhi 110007, India

(Received 31 January 2023; revised 29 June 2023; accepted 29 June 2023)

Terahertz (THz) field excitation by a rotating relativistic electron beam in a magnetized plasma column is described using numerical analysis and particle-in-cell simulation. A rotating electron beam propagating through a cylindrical plasma column excites plasma wakefields. The plasma wakefields couple with the electron beam to excite transverse currents at THz frequency. As a result, the energy of the wakefield directly converts into the form of electromagnetic radiation in the THz range. The magnetic field supports the transverse modes via electron cyclotron resonance. The strength of the THz field is enhanced due to scattering of the spiralling electron beam on the plasma density perturbation. The THz field amplitude is controllable by the electron beam velocity and beam density. On increasing the beam current, the THz field is enhanced significantly. The analytical results are compared with particle-in-cell simulations and are found to be in reasonable agreement.

Key words: intense particle beams, plasma nonlinear phenomena

1. Introduction

Terahertz (THz) radiation generation has emerged as a promising and rapidly developing areas of research in science and engineering, including security and medical diagnostics (Ferguson & Zhang 2002; Dragoman & Dragoman 2004; Taylor *et al.* 2011; Hirori & Tanaka 2013; Lewis 2014; Hafez *et al.* 2016). Vacuum electronic devices (VEDs), such as travelling-wave tubes, have been used to generate high frequencies (Booske *et al.* 2011; Chattopadhyay 2011; Srivastava 2015). But VEDs are difficult to fabricate with the conventional tube technologies because of small dimensions of parts of the radio-frequency circuit being at THz frequencies. The plasma accelerator development (Gupta & Suk 2007; Jain & Gupta 2021; Shpakov *et al.* 2021) solves this problem by creating relatively compact electron beam sources that can generate a THz field in various ways (Sheng, Mima & Zhang 2005; Gupta *et al.* 2022).

Recent research shows the generation of high-charge electron beams using various methods. The availability of high-current electron beams opens new ways to generate low-cost THz sources (Wu *et al.* 2007). The interaction of high-current electron beams with a plasma is one of the promising methods for THz field generation

† Email address for correspondence: dngupta@physics.du.ac.in

(Nikiforov *et al.* 2021). A relativistic electron beam propagating through a plasma can excite electron plasma oscillations via the action of the ponderomotive force. These oscillations are able to convert their energy into the THz field under density gradients or external magnetic fields. For a typical underdense plasma density, the frequencies of these oscillations lie in the THz range. Several methods have been investigated for this study (Jha *et al.* 2005; Maity *et al.* 2021).

In this paper, we investigate a novel radiation scheme, which uses a rotating (spiralling) electron beam to excite THz radiation in a cylindrical plasma column. A cylindrical plasma column is considered, which is immersed in a longitudinal magnetic field. The electron beam propagation in the plasma supports a variety of electrostatic/electromagnetic modes (Sharma 1997; Gupta & Sharma 2004). The proposed mechanism is based on plasma wakefield-mode excitation (Caldwell *et al.* 2010; Zhang *et al.* 2016) by a rotating electron beam. The rotating electron beam excites the transverse wakefield component via radial density perturbation. The magnetic field supports the excited wakefield modes to generate transverse currents at THz frequency. The currents associated with the transverse plasma wakefields generate THz fields. The advantage of this mechanism is to utilize the high beam current to enhance the THz field. Using a simple fluid model, a THz field has been calculated via wakefield excitation. Numerical as well as particle-in-cell (PIC) simulations results are obtained to validate the proposed idea.

The paper is organized as follows: using a simple fluid model, the plasma mode analysis for a rotating electron beam is formulated in § 2. The propagation of a rotating electron beam in a plasma in the presence of a magnetic field is given in § 3. The plasma wakefield excitation and the corresponding transverse wakefield component have been analysed. Numerical results for THz field estimation are presented for the proposed theoretical model. In § 4, we provide PIC simulation results to validate the model. Finally, a conclusion is given in the last section of this paper.

2. Plasma mode analysis

Consider a cylindrical column of radius a. This cylindrical column is filled with a plasma of density n_e. The plasma in this cylindrical plasma column is supported by a longitudinal magnetic field B_s. A rotating electron beam is launched axially to this column for plasma interaction. Consider the plasma equilibrium is perturbed by an electrostatic perturbation with electrostatic potential given by

$$\phi = \phi(r)\exp[-\iota(\omega t - \beta\theta - k_z z)], \tag{2.1}$$

where $\phi(r) = -(n_{0b}(r)e/\epsilon_0 k_z^2)$, β is the azimuthal mode number, ϵ_0 is electric permittivity of free space, $k = \hat{z}k_z$ is the propagation vector, e is the electron charge, ω is the angular frequency of the perturbation and θ is the angular co-ordinate. The electron beam density profile is taken as $n_{0b}(r) = (N_0^0/2\pi a)\delta(r-a)$, where N_0^0 is the number of beam electrons per unit axial length, δ is the Dirac delta function. The static magnetic field is applied along the z-direction as $\boldsymbol{B}_s \parallel \hat{z}$.

The response of plasma electrons to the fields can be governed by the equation of motion

$$m\frac{\mathrm{d}\boldsymbol{V}}{\mathrm{d}t} = e\nabla\phi - e(\boldsymbol{V}\times\boldsymbol{B}_s) \tag{2.2}$$

and the continuity equation

https://doi.org/10.1017/S0022377823000685 Published online by Cambridge University Press

$$\frac{\partial n}{\partial t} + \nabla \cdot nV = 0. \tag{2.3}$$

The linearization of these equations gives the velocity and density perturbations as (Liu and Tripathi 1994)

$$V_{1\perp e} = \frac{e}{m}\frac{\nabla_\perp \phi \times \boldsymbol{\omega}_c + \iota\omega\nabla_\perp\phi}{\omega^2 - \omega_c^2}, \tag{2.4}$$

$$V_{1z} = \frac{-ek_z\phi}{m\omega}, \tag{2.5}$$

$$n_{1e} = -\frac{n_0^0 e}{m}\left(-\frac{\nabla_\perp^2\phi}{\omega^2-\omega_c^2} + \frac{k_z^2\phi}{\omega^2}\right), \tag{2.6}$$

where $-e$ and m are the electron charge and mass, respectively. The sign $\perp$ indicates the direction perpendicular to the magnetic field. Here, the electron cyclotron frequency is defined as $\omega_c = eB_s/m$.

The electrostatic potential excited in the plasma can be obtained using Poisson's equation. We write Poisson's equation in cylindrical coordinates (assuming $\partial/\partial z = 0$) as

$$\frac{\partial^2\phi(r)}{\partial r^2} + \frac{1}{r}\frac{\partial\phi(r)}{\partial r} + \frac{1}{r^2}\frac{\partial^2\phi(r)}{\partial\theta^2} = -\frac{\rho_1}{\epsilon_0}, \tag{2.7}$$

where ρ_1 is the charge density associated with the electron density given by (2.6). Using (2.6) in (2.7), we get

$$\frac{\partial^2\phi(r)}{\partial r^2} + \frac{1}{r}\frac{\partial\phi(r)}{\partial r} + \left(\frac{\left(\frac{\omega_p^2}{\omega^2}-1\right)k_z^2}{\left(1-\frac{\omega_p^2}{\omega^2-\omega_c^2}\right)} - \frac{\beta^2}{r^2}\right)\phi(r) = 0, \tag{2.8}$$

where $\omega_p^2 = n_e e^2/\epsilon_0 m$.

The solution of above equation can be considered as

$$\phi(r) = \alpha\Gamma_{\beta,n}J_\beta(pr), \tag{2.9}$$

where $\Gamma_{\beta,n} = [(2/a^2)J_{\beta+1}^2(p_n a)]^{1/2}$ is the normalization constant such that ϕ must vanish at $r = a$; thus, $(J_\beta(pa) = 0)$. Here, $p = p_n = \chi_n/a$ (with $n = 1, 2, 3$), where χ_n is the zeroth of the Bessel function $J_\beta(x)$.

The electrostatic potential excited in a plasma can be given by (2.9). The expression of different modes of the excited potentials can be obtained using different orders of the Bessel function. In a cylindrical geometry, plasma can support various modes of plasma potential due to geometry effects. This can be seen from the results shown in figure 1. Figure 1 shows the electrostatic potential ($\phi(r)$ in a.u.) of the plasma modes supported in a magnetized plasma column. The solution shown by (2.9) shows that the potential of plasma mode characterizes the extent of localization of the plasma mode and increases with ω/ω_p. This means that the potential of the plasma modes is more strongly localized near ω_p, which can support the excitation of electromagnetic fields by coupling with the spiralling electron beam in the presence of a magnetic field. We study the coupling of plasma modes with the electron beam for THz field excitation in the next section.

https://doi.org/10.1017/S0022377823000685 Published online by Cambridge University Press

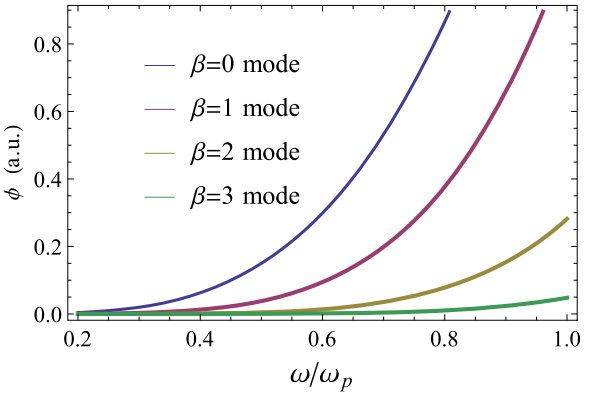

FIGURE 1. Potential of plasma mode for different azimuthal quantum numbers $\beta = 0$, $\beta = 1$, $\beta = 2$, $\beta = 3$ with normalization constant $\alpha = 2 \times 10^6\,\mathrm{V\,cm^{-1}}$, plasma column radius $a = 3.6 \times 10^{-4}\,\mathrm{cm}$, $n_b = 16 \times 10^{16}\,\mathrm{cm^{-3}}$ and $n_e = 8 \times 10^{16}\,\mathrm{cm^{-3}}$.

3. The THz field generation

We consider the propagation of an electron beam of density n_{0b} and velocity V_b with spreading in the azimuthal direction. The beam acquires an oscillatory velocity due to the excited plasma modes. The governing equation for electron motion in the presence of an electron beam can be written as

$$m\frac{\mathrm{d}}{\mathrm{d}t}(\gamma \boldsymbol{V}) = e\nabla\phi - \frac{e}{c}(\boldsymbol{V} \times \boldsymbol{B}_s), \tag{3.1}$$

where $\gamma = (1 - V^2/c^2)^{-(1/2)}$, c is the velocity of light in vacuum.

We solve the above equation by using the perturbation approach in the relativistic regime. The physical quantities are expanded in the form of power series expansions in term of fields. We expressed these expansions as $X = X^{(0)} + \sum_{n=1}^{\infty} \alpha^{(l+1)} X^{(n)}$, where $X = (v)$ and $X^{(0)} = (1)$. Here, α is a normalized parameter which defines the scale of nonlinearity. The source of nonlinearity is the beam electric field for this calculation, hence, α can be expressed in terms of the beam electric field. We apply a first-order perturbation to obtain the perturbed electron velocity as $\boldsymbol{V} = \boldsymbol{V}_{0b} + \boldsymbol{V}_{1b}$. Here, subscript b is for the beam and $\boldsymbol{V}_{1b}$ has components $\boldsymbol{V}_r$ and $\boldsymbol{V}_\theta$.

To obtain the perturbed quantities, we use $\gamma = \gamma_0 + \gamma_0^3 \boldsymbol{V}_{0b} \cdot \boldsymbol{V}_{1z}/c^2$ and $n = n_{0b} + n_{1b}$, where $\boldsymbol{V}_{1br} = -\iota(\bar{\omega} - q\omega_c/\gamma_0)\boldsymbol{r}_1$, $\boldsymbol{V}_{1b\theta} = \boldsymbol{r}_1(\omega_c/\gamma_0) + \boldsymbol{r}_0\dot{\boldsymbol{\theta}}_1$, $\boldsymbol{V}_{1bz} = -\iota(\bar{\omega} - \beta\omega_c/\gamma_0)\boldsymbol{z}_1$ with

$$\boldsymbol{r}_1 = -\frac{e}{m_b}\frac{\left[\gamma_0\left(\bar{\omega} - \dfrac{\beta\omega_c}{\gamma_0}\right)\boldsymbol{E}_{1r} - \iota\left(\dfrac{\omega_c}{\gamma_0}\right)\boldsymbol{E}_{1\theta}\right]}{\left(\bar{\omega} - \dfrac{\beta\omega_c}{\gamma_0}\right)\left[\dfrac{\omega_c^2}{\gamma_0^2} - \gamma_0^2\left(\bar{\omega} - \dfrac{\beta\omega_c}{\gamma_0}\right)^2\right]}, \tag{3.2}$$

$$\boldsymbol{\theta}_1 = -\frac{e}{m_b\boldsymbol{r}_0}\frac{\left[\gamma_0\left(\bar{\omega} - \dfrac{\beta\omega_c}{\gamma_0}\right)\boldsymbol{E}_{1\theta} + \iota\left(\dfrac{\omega_c}{\gamma_0}\right)\boldsymbol{E}_{1r}\right]}{\left(\bar{\omega} - \dfrac{\beta\omega_c}{\gamma_0}\right)\left[\dfrac{\omega_c^2}{\gamma_0^2} - \gamma_0^2\left(\bar{\omega} - \dfrac{\beta\omega_c}{\gamma_0}\right)^2\right]}, \tag{3.3}$$

https://doi.org/10.1017/S0022377823000685 Published online by Cambridge University Press

$$z_1 = -\frac{e\boldsymbol{E}_{1z}}{m_b\gamma_0^3\left(\bar{\omega} - \dfrac{q\omega_c}{\gamma_0}\right)^2}, \tag{3.4}$$

where $\bar{\omega} = \omega - k_z V_{0\|}$.

Solving the equation of continuity $\partial n/\partial t + \nabla \cdot (n\boldsymbol{V}) = 0$, one obtains

$$n_{1b} = \frac{n_{0b}\boldsymbol{k}_z \cdot \boldsymbol{V}_{1b}}{\omega}. \tag{3.5}$$

Now the perturbed current density can be written as

$$\boldsymbol{J}_{1b} = -e(n_{1b}\boldsymbol{V}_{0b} + n_{0b}\boldsymbol{V}_{1b}). \tag{3.6}$$

We define $\boldsymbol{E}_T$ and $\boldsymbol{H}_T$ as THz field structures in the absence of a beam. In the presence of a beam current, let the fields be $\boldsymbol{E} = A_1(t)\boldsymbol{E}_T$ and magnetic field $\boldsymbol{B} = A_2(t)\boldsymbol{B}_T$. Here, the subscript T is used for THz. The above fields satisfy the following Maxwell's equations:

$$\nabla \times \boldsymbol{E} = -\frac{1}{c}\frac{\partial \boldsymbol{B}}{\partial t}, \tag{3.7}$$

$$\nabla \times \boldsymbol{B} = \frac{4\pi}{c}\boldsymbol{J}_{1b} + \frac{\epsilon}{c}\frac{\partial \boldsymbol{E}}{\partial t}. \tag{3.8}$$

Here, $\epsilon = 1 - \omega_p^2/\omega^2$.

Using the above solutions in (3.7) and (3.8), we obtain

$$\frac{\partial A_2}{\partial t} = -\iota\omega(A_1 - A_2), \tag{3.9}$$

$$\left[\epsilon\frac{\partial A_1}{\partial t} - \iota\omega\epsilon(A_1 - A_2)\right]\boldsymbol{E}_T = -4\pi\boldsymbol{J}_{1b}. \tag{3.10}$$

Solving (3.9) and (3.10), assuming $\partial A_1/\partial t \approx \partial A_2/\partial t$ (for high-frequency electromagnetic radiation), we obtain

$$-2\iota\epsilon\omega(A_1 - A_2)\boldsymbol{E}_T = -4\pi\boldsymbol{J}_{1b}. \tag{3.11}$$

Taking the dot product of this equation by $\boldsymbol{E}_T r\,\mathrm{d}r$ and integrating over r from 0 to ∞, we get

$$\frac{\partial A_1}{\partial t} = \frac{2\pi}{\epsilon}\frac{\displaystyle\int_0^\infty \boldsymbol{J}_{1bz}\boldsymbol{E}_{Tz}^* r\,\mathrm{d}r}{\displaystyle\int_0^\infty \boldsymbol{E}_T \cdot \boldsymbol{E}_T^* r\,\mathrm{d}r}. \tag{3.12}$$

https://doi.org/10.1017/S0022377823000685 Published online by Cambridge University Press

By simplifying, we get all components of the generated THz electric field as follows:

$$\boldsymbol{E}_{Tr} = \frac{2\pi e^2 n_{0b} l}{\omega \epsilon m_b (A_1 - A_2)} \left(\frac{\boldsymbol{k}\boldsymbol{V}_{0b}}{\omega} + 1\right) \frac{\left[\gamma_0 \left(\bar{\omega} - \frac{\beta\omega_c}{\gamma_0}\right) \nabla\phi_r + \iota \left(\frac{\omega_c}{\gamma_0}\right) \nabla\phi_\theta\right]}{\left[\frac{\omega_c^2}{\gamma_0^2} - \gamma_0^2 \left(\bar{\omega} - \frac{\beta\omega_c}{\gamma_0}\right)^2\right]}, \tag{3.13}$$

$$\boldsymbol{E}_{T\theta} = \frac{2\pi \iota e^2 n_{0b}}{\omega \epsilon m_b (A_1 - A_2) \left(\bar{\omega} - \frac{\beta\omega_c}{\gamma_0}\right) \left[\frac{\omega_c^2}{\gamma_0^2} - \gamma_0^2 \left(\bar{\omega} - \frac{l\omega_c}{\gamma_0}\right)^2\right]} \left(\frac{\boldsymbol{k}\boldsymbol{V}_{0b}}{\omega} + 1\right)$$
$$\times \left[\omega_c \left(\bar{\omega} - \frac{\beta\omega_c}{\gamma_0}\right) \nabla\phi_r + \iota \frac{\omega_c^2}{\gamma_0^2} \nabla\phi_\theta + \iota\omega(-\gamma_0) \left(\bar{\omega} - \frac{\beta\omega_c}{\gamma_0}\right) \nabla\phi_\theta - \iota \frac{\omega_c}{\gamma_0} \nabla\phi_r\right], \tag{3.14}$$

$$\boldsymbol{E}_{Tz} = -\frac{2\pi e^2 n_{0b}}{\omega \epsilon m_b \gamma_0^3 (A_1 - A_2)} \frac{\left(\frac{\boldsymbol{k}\boldsymbol{V}_{0b}}{\omega} + 1\right)}{\left(\bar{\omega} - \frac{\beta\omega_c}{\gamma_0}\right)} \nabla\phi_z. \tag{3.15}$$

Equations (3.13)–(3.15) show the excited electromagnetic fields generated by the spiral electron beam interaction with a plasma. We estimate the transverse component of the electromagnetic field (THz field) for various electron beam parameters. The dependency of the excited THz fields on the electron beam velocity and electron beam density is illustrated in figure 2. Figure 2(*a*) shows the spectral variation of the THz field (in GV m^{-1}) for different electron beam velocities. The results depicted in figure 2(*a*) show that the beam velocity plays an important role in THz field excitation. The THz field increases with the electron beam velocity due to large transverse current generation during the electron beam interaction with plasmas. The large beam velocity obviously contributes profoundly to the transverse current density because the current density is directly proportional to the charge carrier velocity. Thus, the THz field strength is enhanced by the beam velocity, as confirmed by these results. We know that the THz field peaks near ω_p due to resonance. Our results shows that the THz field is maximized near ω_p, as shown in the results of figure 2. The deviation in plasma frequency diverts the pump energy, hence, the transverse current may be varied accordingly. On the other hand, the applied magnetic field supports the transverse oscillations, which contribute via electron cyclotron resonance. Figure 2(*b*) shows the spectral distribution of the THz field for different beam velocities. It is clear from (3.13) that the radial electric field increases with the beam velocity. Consequently, the THz field increases with the beam velocity. The higher electron beam density enhances the plasma oscillations via strong excitation of the plasma density perturbation. In a result, the transverse current associated with the plasma oscillations will be stronger for the large beam density. A stronger peak THz field for the large beam density can be confirmed from the results shown in figure 2(*b*).

4. The PIC simulation results

To validate the proposed theoretical model, we carried out quasi-three-dimensional (quasi-3-D) simulations. In this study, we investigate THz field generation using the interaction of an electron beam with a plasma in a cylindrical column. For this study, these simulations are performed using the spectral, quasi-3-D PIC code FBPIC (Lehe

https://doi.org/10.1017/S0022377823000685 Published online by Cambridge University Press

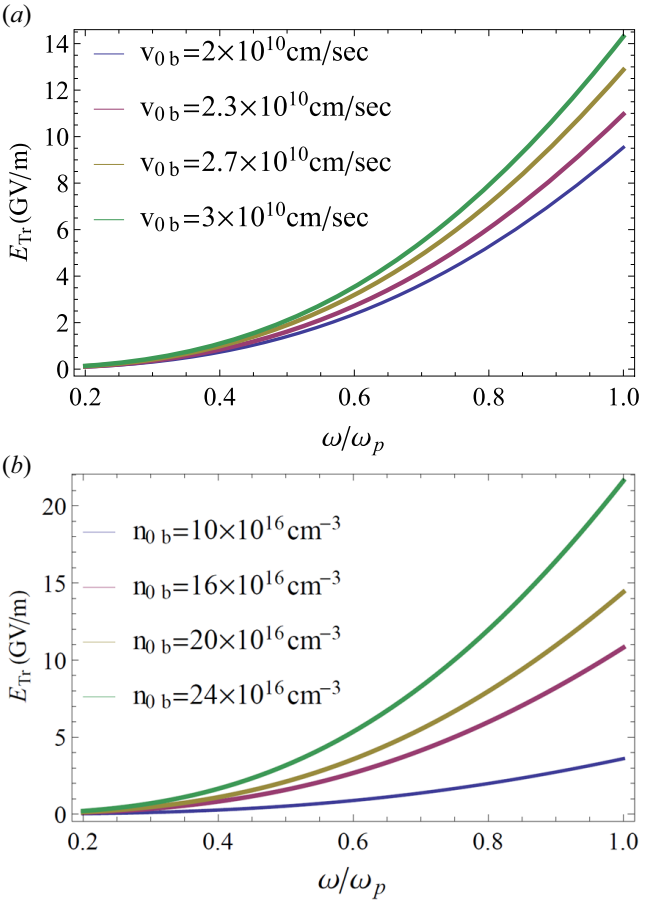

FIGURE 2. Spectral distribution of THz field (in $\mathrm{GV\,m^{-1}}$) for (*a*) different electron beam velocities $V_{0b} = 2 \times 10^{10}\,\mathrm{cm\,s^{-1}}$, $V_{0b} = 2.3 \times 10^{10}\,\mathrm{cm\,s^{-1}}$, $V_{0b} = 2.7 \times 10^{10}\,\mathrm{cm\,s^{-1}}$, $V_{0b} = 3 \times 10^{10}\,\mathrm{cm\,s^{-1}}$ with $n_e = 8 \times 10^{16}\,\mathrm{cm^{-3}}$, $n_{0b} = 16 \times 10^{16}\,\mathrm{cm^{-3}}$ and (*b*) different electron beam densities $n_{0b} = 10 \times 10^{16}\,\mathrm{cm^{-3}}$, $n_{0b} = 16 \times 10^{16}\,\mathrm{cm^{-3}}$, $n_{0b} = 20 \times 10^{16}\,\mathrm{cm^{-3}}$, $n_{0b} = 24 \times 10^{16}\,\mathrm{cm^{-3}}$ with $n_e = 8 \times 10^{16}\,\mathrm{cm^{-3}}$. The plasma is filled in a plasma column of radius $a = 3.6 \times 10^{-4}\,\mathrm{cm^{-1}}$ with a magnetic field of 0.1 T.

et al. 2016). This code uses a spectral cylindrical representation, which decreases the computational load in the laser interaction process. FBPIC contains a set of 2-D radial grids which represents an azimuthal mode. The fields are decomposed into two azimuthal modes ($N_m = 2$). The simulation grid size is set to be $0.14\,\mu\mathrm{m} \times 0.4\,\mu\mathrm{m}$ in the longitudinal and transverse directions, respectively (with 8 particles per cell). The moving window with size $170\,\mu\mathrm{m} \times 60\,\mu\mathrm{m}$ is large enough to simulate plasma oscillations in the first cycle. The parameters for an electron beam used in the simulations are as follows: beam size ($\sigma_r = 5\,\mu\mathrm{m}$, $\sigma_z = 10\,\mu\mathrm{m}$), beam energy 28 GeV and beam density range is $n_b =$ 16–24 $\times\ 10^{16}\,\mathrm{cm^{-3}}$. The plasma density taken for these simulations is $n_e = 8 \times 10^{16}\,\mathrm{cm^{-3}}$ with a magnetic field of 0.1 T.

Figure 3 shows the PIC simulation results of the THz field excitation corresponding to the theoretical model given § 3. The excited THz field and the corresponding transverse current density both are given in this figure. The average low-frequency ponderomotive

https://doi.org/10.1017/S0022377823000685 Published online by Cambridge University Press

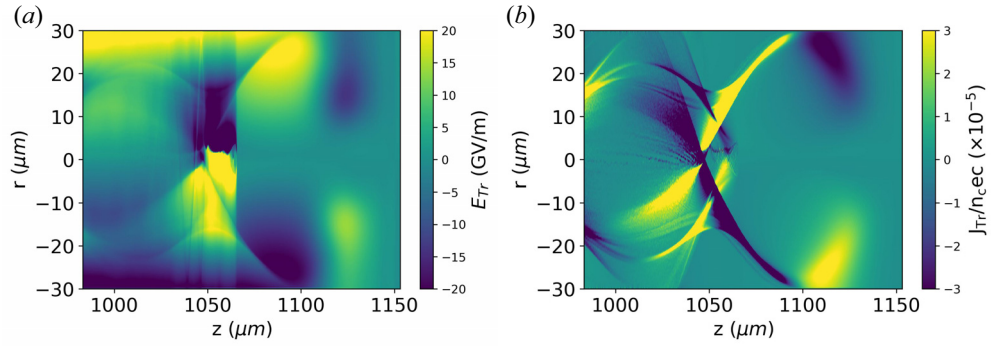

FIGURE 3. Snapshots of (*a*) THz electric field E_{Tr} (GV m^{-1}) and (*b*) transverse current density J_x (normalized by $n_c ec$, where $n_c = 10^{21}\lambda_0^{-2}$ cm^{-3} is the critical plasma density) for $n_b = 24 \times 10^{16}$ cm^{-3}.

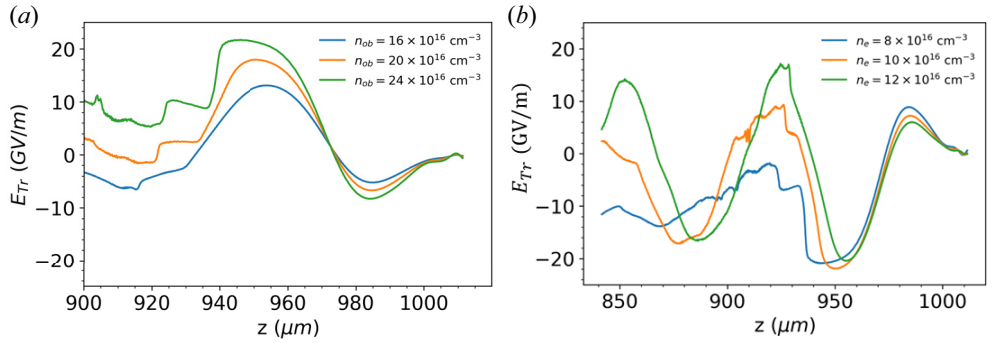

FIGURE 4. Simulation results of THz electric field E_{Tr} (GV m^{-1}) for different (*a*) electron beam densities with $n_e = 8 \times 10^{16}$ cm^{-3} and (*b*) plasma densities n_e with $n_{0b} = 24 \times 10^{16}$ cm^{-3}. The other numerical parameters are same as those of figure 3.

force associated with the electron beam drives plasma oscillations, generating a dynamic plasma current. The finite rotation of the electron beam generates a transverse component of this current, which excites THz radiation. It is evident from the simulation results that the transverse plasma current is generated by a rotating electron beam while interacting with the plasma. Thus the corresponding THz field is finite. To clearly demonstrate the role of the electron beam parameters, we have depicted the THz field evolution in figure 4 for different beam densities and plasma densities. These results are obtained from the simulation data.

THz field increases with the electron beam density, as predicted previously by the theoretical model. The PIC simulation results show that the maximum THz field is approximately 10 GV m^{-1} for the electron beam density of $n_{0b} = 16 \times 10^{16}$ cm^{-3}. This value of the peak THz field is also very close to the data obtained from the theoretical model (see figure 2*b*). This peak THz field corresponds to the resonance condition ($\omega \approx \omega_p$). The peak THz field also depends on the plasma density. The maximum THz field is enhanced by the plasma density. The peak THz field position is also shifted due to the variation of ω_p, as seen in figure 4(*b*). The radiation field is peaked at ω_p for a given plasma density. Thus, the peak radiation field is tuneable with the beam density and velocity. These simulation results are consistent with the theoretical findings. However, a

https://doi.org/10.1017/S0022377823000685 Published online by Cambridge University Press

deviation in the THz field profile can be observed as the simulation results are inconsistent with the envelope model.

5. Conclusion

We have investigated a way to generate THz fields by employing a rotating electron beam for plasma interaction with a cylindrical plasma column. The mechanism is based on transverse plasma current generation by a spiralling electron beam. We have described a systematic theoretical model for this mechanism. The obtained results are in fairly good agreement with quasi-3-D PIC simulation results. It was found that the radial extent of the rotating electron beam can sustain the transverse motion of the plasma electrons, which can excite transverse electromagnetic fields in the THz frequency range. We reported a substantial increase in the THz field, as high as $10\,\mathrm{GV\,m^{-1}}$, by employing a rotating electron beam. Scaling laws have also been obtained for THz field optimization. The THz field is tuneable by the electron beam parameters. Such a compact source of THz radiation not only triggers various nonlinear dynamics in matter, but also opens up the research era of relativistic THz optics.

Acknowledgements

The authors would like to thank the Department of Physics and Astrophysics, University of Delhi, India for providing computational facilities to carry out the numerical work. This work was financially supported by the Science and Engineering Research Board, Department of Science and Technology, Government of India (Grant No. CRG/2022/001989 and INT/RUS/RFBR/394) and the Institution of Eminence (IoE), University of Delhi under Faculty Research Programme Grant (Ref. No. IoE/2021/12/FRP).

Editor Victor Malka thanks the referees for their advice in evaluating this article.

Declaration of interests

The authors report no conflict of interest.

REFERENCES

Booske, J.H., Dobbs, R.J., Joye, C.D., Kory, C.L., Neil, G.R., Park, G., Park, J. & Temkin, R.J. 2011 Vacuum electronic high power terahertz sources. *IEEE Trans. Terahertz Sci. Technol.* **1**, 54.

Caldwell, A., Lotov, K., Pukhov, A. & Xia, G. 2010 Plasma wakefield excitation with a 24 gev proton beam. *Plasma Phys. Control. Fusion* **53** (1), 014003.

Chattopadhyay, G. 2011 Technology, capabilities, and performance of low power terahertz sources. *IEEE Trans. Terahertz Sci. Technol.* **1** (1), 33–53.

Dragoman, D. & Dragoman, M. 2004 Terahertz fields and applications. *Prog. Quant. Electron.* **28** (1), 1–66.

Ferguson, B. & Zhang, X.-C. 2002 Materials for terahertz science and technology. *Nat. Mater.* **1** (1), 26–33.

Gupta, D.N., Jain, A., Kulagin, V.V., Hur, M.S. & Suk, H. 2022 Coherent terahertz radiation generation by a flattened gaussian laser beam at a plasma–vacuum interface. *Appl. Phys.* B **128**, 50.

Gupta, D.N. & Sharma, A.K. 2004 Parametric up-conversion of a trivelpiece–gould mode in a beam–plasma system. *Laser Part. Beams* **22** (1), 89–94.

Gupta, D.N. & Suk, H. 2007 Energetic electron beam generation by laser-plasma interaction and its application for neutron production. *J. Appl. Phys.* **101** (11), 114908.

Gurjar, M.C., Gopal, K., Gupta, D.N. & Kulagin, V.V. 2021 Terahertz radiation generation from short-pulse laser interaction with electron-hole plasmas. *Europhys. Lett.)* **133** (1), 14001.

Gurjar, M.C., Gopal, K., Gupta, D.N., Kulagin, V.V. & Suk, H. 2020 High-field coherent terahertz radiation generation from chirped laser pulse interaction with plasmas. *IEEE Trans. Plasma Sci*. **48** (10), 3727–3734.

Hafez, H.A., Chai, X., Ibrahim, A., Mondal, S., Férachou, D., Ropagnol, X. & Ozaki, T. 2016 Intense terahertz radiation and their applications. *J. Opt*. **18** (9), 093004.

Hirori, H. & Tanaka, K. 2013 Nonlinear optical phenomena induced by intense single-cycle terahertz pulses. *IEEE J. Sel. Top. Quantum. Electron*. **19**, 8401110.

Jain, A. & Gupta, D.N. 2021 Optimization of electron bunch quality using a chirped laser pulse in laser wakefield acceleration. *Phys. Rev. Accel. Beams* **24**, 111302.

Jha, P., Kumar, P., Upadhyaya, A.K. & Raj, G. 2005 Electric and magnetic wakefields in a plasma channel. *Phys. Rev*. **8** (7), 071301.

Lehe, R., Kirchen, M., Andriyash, I.A., Godfrey, B.B. & Vay, J.L. 2016 A spectral, quasi-cylindrical and dispersion-free Particle-In-Cell algorithm. *Comput. Phys. Commun*. **203**, 66–82.

Lewis, R.A. 2014 A review of terahertz sources. *J. Phys.* D*: Appl. Phys*. **47**, 374001.

Liu, C.S. & Tripathi, V.K. 1994 *Interaction of Electromagnetic Waves with Electron Beams and Plasmas*. World Scientific.

Maity, S., Mandal, D., Vashistha, A., Goswami, L.P. & Das, A. 2021 Harmonic generation in the interaction of laser with a magnetized overdense plasma. *J. Plasma Phys*. **87** (5), 905870509.

Nikiforov, D.A., Petrenko, A.V., Sinitsky, S.L., Bak, P.A., Skovorodin, D.I., Logachev, P.V., Zhivankov, K.I., Sandalov, E.S., Meshkov, O.I., Ivanov, A.V., Starostenko, D.A., Nikitin, O.A., Akhmetov, A.R., *et al.* 2021 Investigation of high current electron beam dynamics in linear induction accelerator for creation of a high-power THz radiation source. *J. Instrum.* **16**, 11024.

Sharma, S.C. 1997 Excitation of upper-hybrid waves by a rotating relativistic electron beam in a plasma-filled large-orbit gyrotron. *J. Plasma Phys*. **57** (3), 545–553.

Sheng, Z.M., Mima, K. & Zhang, J. 2005 Powerful terahertz emission from laser wake fields excited in inhomogeneous plasmas. *Phys. Plasmas* **12** (12), 123103.

Shpakov, V., Anania, M.P., Behtouei, M., Bellaveglia, M., Biagioni, A., Cesarini, M., Chiadroni, E., Cianchi, A., Costa, G., Croia, M., *et al.* 2021 First emittance measurement of the beam-driven plasma wakefield accelerated electron beam. *Phys. Rev. Accel. Beams* **24** (5), 051301.

Srivastava, V. 2015 Vacuum microelectronic devices for THz communication systems. In *2015 Annual IEEE India Conference*, pp. 1–5. IEEE. doi: 10.1109/INDICON.2015.7443109.

Taylor, Z.D., Singh, R.S., Bennett, D.B., Tewari, P., Kealey, C.P., Bajwa, N., Culjat, M.O., Stojadinovic, A., Lee, H., Hubschman, J.-P., *et al.* 2011 Thz medical imaging: in vivo hydration sensing. *IEEE Trans. Terahertz Sci. Technol*. **1** (1), 201–219.

Wu, H.-C., Sheng, Z.-M., Dong, Q.-L., Xu, H. & Zhang, J. 2007 Powerful terahertz emission from laser wakefields in inhomogeneous magnetized plasmas. *Phys. Rev.* E **75** (1), 016407.

Zhang, G.-B., Chen, M., Schroeder, C.B., Luo, J., Zeng, M., Li, F.-Y., Yu, L.-L., Weng, S.-M., Ma, Y.-Y., Yu, T.-P., *et al.* 2016 Acceleration and evolution of a hollow electron beam in wakefields driven by a Laguerre-Gaussian laser pulse. *Phys. Plasmas* **23** (3), 033114.